First published in *Physics in Medicine and Biology,* volume 50, issue 20 (2005).
Published by The Institute of Physics Publishing Ltd

Application of the lattice Boltzmann model to simulated stenosis growth in a two dimensional carotid artery.

J Boyd[†], J Buick[†], J A Cosgrove[‡] and P Stansell[‡]

[†] Biophysical and Biomedical Research Group, School of Biological, Biomedical and Molecular Sciences, University of New England, Armidale, NSW, 2351, Australia

[‡] School of Physics, University of Edinburgh, Edinburgh, Scotland, UK

Abstract

The lattice Boltzmann model is used to observe changes in the velocity flow and shear stress in a carotid artery model during a simulated stenosis growth. Near wall shear stress in the unstenosed artery is found to agree with literature values.

The model also shows regions of low velocity, rotational flow and low near wall shear stress along parts of the walls of the carotid artery that have been identified as being prone to atherosclerosis. These regions persist during the simulated stenosis growth, suggesting that atherosclerotic plaque build up creates regions of flow with properties that favour atherosclerotic progression.

1 Introduction

There is a body of evidence that suggests a correlation between atherosclerosis, regions of low blood flow velocity, rotational flow and low shear stress near the walls of arteries (Malek *et al.* 1999, Asakure and Karino 1990, Gnasso *et al.* 1997). Therefore the study of the haemodynamic properties of the blood flow in these regions of the artery can lead to a greater understanding of atherosclerosis and its dependence on flow parameters. However, accurate measurements of quantities of interest, such as shear stress, are difficult to make *in vivo*, thus numerical simulation becomes a valuable investigative tool.

The lattice Boltzmann model (LBM) uses a simplified kinetic equation to simulate fluid flow and has been applied to many general problems including turbulence (Cosgrove *et al.* 2003), magnetohydrodynamics (Chen *et al.* 1991) and multiphase flows (Shan and Chen 1993), as well as in areas relevant to blood flow simulation such as in flows with elastic and moving boundaries (Fang *et al.* 1998), steady and pulsating flow (Fang *et al.* 2002), particle suspensions (Ladd and Verberg 2001), and flows with complex boundaries (Manwart *et al.* 2002, Guo *et al.* 2002). Migliorini *et al.* (2002) consider the forces acting on leukocytes due to red blood cells in a two dimensional simulation of a blood vessel. This work was continued by Sun *et al.* (2003).

It has been applied to a limited number of blood flow simulations. Krafczyk *et al.* (1998, 2001) consider blood flow through an artificial aortic valve. They present details of transient flows at selected fixed openings and also consider a two-dimensional model with moving leaflets. Bellerman and Sloot (2001) propose using the LBM in an ambitious project to build a 'virtual laboratory' in which LBM simulations will be combined with visualisation techniques. Tamagawa and Matsuo (2004) simulate blood flow in a simple model of a blood pump or a medical fluid machine. They further estimate thrombus formation from the shear rate and the effective distance of the wall. Artoli *et al.* (2004) consider a two dimensional model of a symmetric bifurcation and compare the LBM results to a Navier-Stokes solver. The implementation of compliant walls in a two dimensional tube representing a blood vessel was considered by Fang *et al.* (2002) and Hoekstra *et al.* (2004). Li *et al.* (2004, 2005) consider the transport of red blood cells through a two dimensional symmetric model of an artery containing a semi-circular stenosis. Measurement of force on moving boundaries and suspended particles has also been investigated (Li *et al.* 2004).

The developments outlined above show that the LBM is suited to simulating a number of features which are important in arterial haemodynamics. For a given simulation, the features that are deemed to be important can be integrated in a realistic model. In some areas, such as the simulation of transport of red blood cells, the LBM offers advantages over alternative numerical approaches. In other areas, such as simulating compliant walls, the LBM approach provides an efficient, validated approach to implementing a feature which can be found in many alternative CFD codes. In the study of haemodynamics the LBM can play an important contribution, as it is doing in other fields of fluid mechanics. The technique can be applied in the same continuum limit as the more traditional Navier-Stokes solvers. Further it can also potentially be applied at the smaller length scales of capillaries (Agarwal *et al.* (2001), Spaid *et al.* (1997), Lim *et al.* (2002), Nie *et al.* (2002)) once its application to larger scales has been fully implemented.

In this paper a two dimensional model of the human carotid artery with a simulated stenosis growth is presented. The simulations are performed using rigid walls. This is a good approximation in the region of the stenosis which is the area of interest here in terms of measuring the wall shear stress. Healthy regions of the artery will exhibit a level of compliance which is not considered here. This will influence the calculated velocity and shear stress field; however, given the two dimensional nature of the simulation and the fact the stenosis shape, size and position varies considerable between patients, the aim of this paper is to investigate how the wall shear varies in the presence of stenosis growth, rather than determining detailed flow fields. The blood

is modelled as a Newtonian fluid. This is generally assumed to be an acceptable approximation for larger vessels, such as the carotid (Quarteroni *et al.* 2000). The stenosis growth is implemented in a region of the internal carotid artery which exhibits low velocity flow and a low near wall shear stress. This region is also one which is commonly prone to atherosclerotic progression. Maximum near wall shear stresses at points in the artery are compared with literature results and changes in the velocity and shear fields due to stenosis growth within the artery are examined. It is found that for the simulated stenosis growth, persistent regions of low velocity and low near wall shear are observed, particularly near the wall upstream from the stenosis growth. This suggests that the plaque build up maintains flow conditions favourable to its progression.

2 Theoretical Background

2.1 The Lattice Boltzmann Method

The lattice Boltzmann method (Chen and Doolen 1998) has recently been developed as an alternative method for simulating a range of fluid flows. In the LBM particle distribution functions, $f_i(\mathbf{x}, t)$ at point $\mathbf{x}$ at time t, are confined to move synchronously on a regular lattice. The distribution functions interact on the lattice in a way that conserves mass, momentum, isotropy and Galilean invariance. Here i labels the lattice link the distribution function is on. The lattice used in this paper is the D2Q9, shown in figure 1.

The evolution of the distribution functions on the lattice is governed by the discrete Boltzmann equation (Chen and Doolen 1998)

$$f_i(\mathbf{x} + \mathbf{e}_i \Delta x, t + \Delta t) = f_i(\mathbf{x}, t) + \Omega_i(\mathbf{x}, t), \qquad (i = 0, 1 \cdots, M), \tag{1}$$

where for the D2Q9 lattice, see figure 1,

$$\begin{array}{rcll} \mathbf{e}_0 & = & (0,0), & ,(i=0), \\ \mathbf{e}_i & = & \left(\cos\left(\frac{\pi}{2}(i-1)\right), \sin\left(\frac{\pi}{2}(i-1)\right)\right) & ,(i=1,2,3,4), \\ \mathbf{e}_i & = & \sqrt{2}\left(\cos\left(\frac{\pi}{2}(i-1)+\frac{\pi}{4}\right), \sin\left(\frac{\pi}{2}(i-1)+\frac{\pi}{4}\right)\right) & ,(i=5,6,7,8), \end{array} \tag{2}$$

and Ω_i is the collision operator. The fluid density ρ and velocity $\mathbf{u}$ can be calculated directly from the distribution functions at each node by

$$\rho = \sum_i f_i \qquad \text{and} \qquad \rho \mathbf{u} = \sum_i f_i \mathbf{e}_i, \tag{3}$$

The collision operator Ω_i is given by the Bhatnagar-Gross-Krook approximation as (Bhatnagar *et al.* 1954, Chen and Doolen 1998)

$$\Omega_i = \frac{-1}{\tau}[f_i(\mathbf{x},t) - f_i^{eq}(\mathbf{x},t)], \tag{4}$$

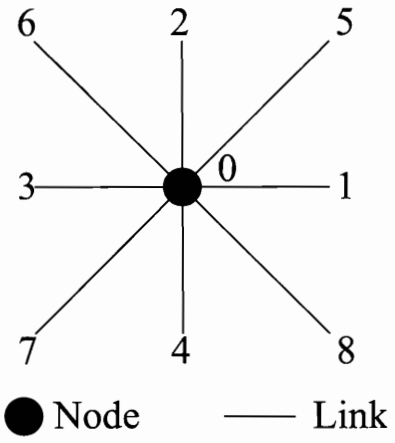

Figure 1: The D2Q9 lattice. The black circle is the node, and the lines are the link directions, numbered from 1-8.

where τ is the relaxation time and $f_i^{eq}(\mathbf{x},t)$ is the equilibrium value of the distribution function.

The equilibrium form of the distribution function in two dimensions for the D2Q9 lattice is given by (Quian *et al.* 1992)

$$f_i^{eq}(\mathbf{x},t) = w_i\rho(1 + 3\mathbf{e}_i \cdot \mathbf{u} + \frac{9}{2}(\mathbf{e}_i \cdot \mathbf{u})^2 - \frac{3}{2}\mathbf{u}^2) \tag{5}$$

where $w_0 = 4/9$, $w_i = 1/9$ for i = 1,2,3,4 and $w_i = 1/36$ for i = 5,6,7,8. The relaxation time τ is related to the kinematic viscosity ν by

$$\nu = \frac{2\tau - 1}{6}. \tag{6}$$

The LBM reproduces the Navier stokes equation in the nearly incompressible limit and is second order accurate in the body of the fluid (Chen and Doolen 1998).

A sub-grid accurate extrapolation boundary scheme (Guo *et al.* 2002) is used to implement the artery geometry in the model. This boundary scheme retains the second order nature of the LBM and is well suited to modelling stenosis growth since it enables the shape of the artery wall and the stenosis

to be modelled at a resolution greater than that provided by the underlying lattice (Boyd *et al.* 2004).

At the entry of the artery a predetermined profile was implemented, this will be described in the following section. This boundary condition was implemented by setting the distribution functions at the entry equal to their equilibrium values, calculated from equation (5, for the desired velocity and density. The profile was applied uniformly across the width of the entry except for a boundary layer region of with approximately 1mm over which the velocity reduced to zero (Boyd *et al.* 2004). It can be seen from figures 2 which shows the geometry of the carotid artery and figure 3 which shows the region of the artery where used to present the results, that the entry position of the computational artery is a significantly distance from the region from which the results were obtained. Small variations in the entry parameters, such as the width of the boundary layer, were not found to make a significant difference to the presented results.

The unknown distribution functions at an exit site $\mathbf{x}$ were found from a linear extrapolation, based on (Neal 2002):

$$f_i(\mathbf{x}, t+1) = 2f_i(\mathbf{x}+\mathbf{e}_i, t+1) - f_i(\mathbf{x}+2\mathbf{e}_i, t+1). \tag{7}$$

Note that the additional constraint of Neal (2002) which should be expressed as:

$$\begin{array}{l} \textbf{if } [\mathbf{e}_i \cdot \mathbf{u}(\mathbf{x}, t+1)][\mathbf{e}_i \cdot \mathbf{u}(\mathbf{x}+\mathbf{e}_i, t+1)] \leq 0 \\ \textbf{then } f_i(\mathbf{x}, t+1) = f_i^{eq}|_{\rho=\rho(\mathbf{x}+\mathbf{e}_i, t+1), \mathbf{u}=\mathbf{0}} \end{array} \tag{8}$$

was not implemented here since there was no change in the sign of the velocity at the exit.

3 Methods and results

Figure 2 shows the carotid artery geometry that was used for the simulation. Thirty incrementally larger stenosis growths were implemented in a region of the artery that exhibited low velocity and low near wall shears and is known to be susceptible to atherosclerosis (Gnasso *et al.* 1997), figure 3. The stenosis geometries were chosen to vary smoothly between increments. A pulsatile waveform, shown in figure 4 adapted from Holdsworth *et al.* (1999), was implemented at the base of the artery. It was found that two pulse periods were sufficient for any transients in the flow to reduce to acceptable levels.

Blood was assumed to be Newtonian, this is generally held to be a good first approximation (McDonald 1960, Quarteroni *et al.* 2000). The kinematic

viscosity of blood was taken to be $\nu = 4 \times 10^{-6}$ m^2 s^{-1}. The artery walls were assumed to be rigid, which is accurate near the vicinity of the stenosis itself (Steinke *et al.* 1994) and a good approximation in a large artery such as the carotid. A grid resolution of 12.5 grid points per mm was implemented and each pulse period corresponded to around 4 million simulation time-steps.

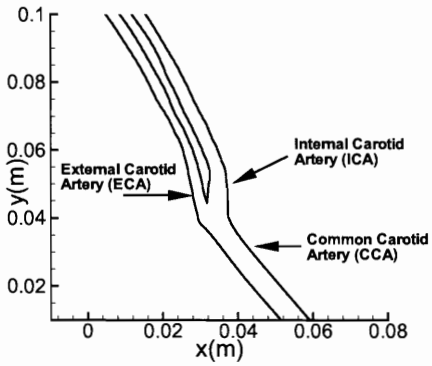

Figure 2: Carotid artery geometry used.

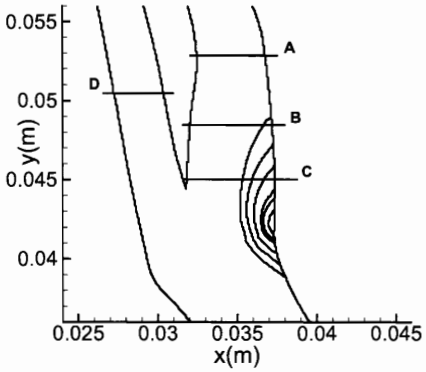

Figure 3: Stenosis implementation, every fifth increment shown. The intersections of lines A-D show the locations of near wall shear measurements taken for comparison with literature values

Figures 5 and 6 show the absolute velocity flow fields (VFF) and shear stress during the simulated stenosis growth in the carotid artery. The unstenosed artery and stenosis increments 10, 15, 20, 25 and 30 are shown. The images were all taken at the time of peak velocity in the unstenosed artery which corresponded to a time of $t = 0.066$ s into the pulse period, figure 4.

Figures 7 and **??** show the changing VFF and shear stress in the maximally stenosed artery at times of $t = 0.05$ s, 0.12 s, 0.17 s, 0.22 s, 0.28 s and 0.50 s. These times were chosen to emphasise changes that occur in the flow characteristics during a pulse cycle.

The primary region of interest is along the lower outer wall of the internal carotid artery (ICA). It can be seen that there is a large region of low velocity flow and corresponding low near wall shear indicating an area prone to atherosclerosis. It was in this region that the simulated stenosis was implemented. A similar region is also observed along the outer wall of the

common carotid artery (CCA).

The shear values at the inner and outer wall indicated by the lines **A-D** in figure 3 were compared to literature values for maximum wall shear obtained from Ku *et al.* (1985) and Perktold *et al.* (1991), shown in table 1. The distribution of the shears and the numerical values qualitatively agree with the literature values. Discrepancies in the values obtained may arise from the 2D nature of the simulation, differences in the arterial geometry, the waveform implemented, the exact location of the measurements and the manner in which they were taken.

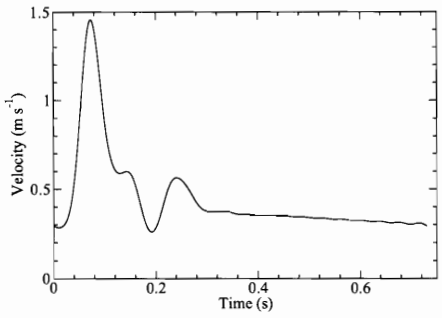

Figure 4: Pulse waveform implemented at the base of the common carotid artery geometry shown in figure 2.

As can be observed from figures 5 and 6, the majority of the shear stress in the artery is concentrated along the walls during the peak velocity. This is also true for the majority of the pulse cycle, as observed in figures 7 and **??**. The largest changes during the simulated stenosis growth occurred near the boundary of the stenosis itself. In order to examine how the near wall shear stress along the boundary of the stenosis changes in response to the stenosis growth, the shear near a section of the wall extending from $y = 0.0384$ m to $y = 0.0496$ m, a total vertical distance of 11.2 mm, encompassing the stenosis boundary was examined.

Whilst the extrapolation schemes allows the LBM to model the carotid artery with a sub-grid boundary, the model only outputs velocity values at nodes within the fluid. Thus to measure near wall shear stress at positions other than those lying on lattice nodes, a form of interpolation is needed. Figure 8 shows interpolated near wall shears measured 0.16 mm from the wall along the selected wall section. This distance is not a limitation of the LBM model, but was selected to enable comparison with literature results where wall shear stress is typically measured some distance from the wall.

Table 1: Wall shear stress comparison with data obtained from Ku *et al.* and Perktold *et al.*. All values are given in Pascals (Pa).

	Inner wall shear (Pa)			Outer wall shear (Pa)		
Axial Position	Ku *et al.*	Perktold *et al.*	Model	Ku *et al.*	Perktold *et al.*	Model
A	10.9	6.74	7.4	4.9	6.48	2
B	4.1	4.18	3.7	1.3	1.92	1.7
C	5	12.58	8.4	0.4	0.88	1.2
D	5.6	-	4.0	3.5	-	6.4

The distance of 0.16 mm corresponds to two grid lengths. Due to the sub-gird boundary resolution, neither the boundary nor the point 2 gird lengths for the boundary as generally at a grid point, thus the need to interpolated the shear values. The small oscillations in the curved are mainly generated by the fact that the interpolation is taken along the links of the lattice, which may not be perpendicular to the boundary. These curves give a good indication of the behaviour of the shear near the wall, and thus a more complicated interpolation scheme is not required.

4 Discussion

4.1 Stenosis Growth

A number of interesting features were observed during the stenosis growth. The region of low velocity flow observed in figure 5(a) is preserved behind the growing stenosis. The corresponding region of low near wall shear is also preserved, particularly along the upper edge of the stenosis.

A small region of slow rotational flow near the outer ICA wall is observed inside the larger region of low velocity flow, indicated by the small shear shown by the arrow in figure 5(d). This rotational flow also persists during the stenosis growth and remains in the area immediately after the upper edge of the stenosis.

The largest changes in carotid artery VFF occur once the stenosis edge penetrates into the central higher velocity flow observed in the unstenosed artery in figure 5(a). This occurs at around increment 15, see figures 5 e) and 6 a). Higher velocities are exhibited in the central region of the artery during maximal stenosis growth, particularly in the upper part of the CCA.

This increase in velocity corresponds to an increase in the near wall shear stress along the lower edge of the stenosis growth. The highest shear along the edge of the stenosis corresponds to the place where the stenosis edge penetrates from the initial low velocity region into the high velocity central flow corresponding to the change in the VFF noted above. A plume of higher shear extends from this point, with the shear increasing as the stenosis grows.

The velocities and shears outside the central region near the stenosis remain relatively unchanged. The shear along the walls of the external carotid artery, the bifurcation and the inner wall of the ICA remain uniformly high. A small region of low velocity and low near wall shear is also preserved along the upper right-hand wall of the CCA. Small rotational flow was also observed in that area, indicating it may also be a region of the artery susceptible to atherosclerosis. This is borne out by the literature (Gnasso *et al.* 1997).

Along the wall of the stenosis, it can be seen that as the stenosis grows, two regions of higher shear stress develop. The high shear stress that develops in the lower portion of the wall is centered around $y = 0.042$ m. This region of high shear stress corresponds to the portion of the stenosis wall which is closest to the interface between the central high velocity flow and the region of low velocity flow seen in figures 5 and 6. The wall shear stress in this portion of the stenosis boundary increases with the stenosis growth, the length of the boundary wall which is subject to the higher shear stresses also increases with the stenosis growth.

The second region of high wall shear stress is initially centered around $y = 0.0456$ m. As the stenosis grows, this region of high shear stress moves up the artery wall. During the initial stages of growth, this shear stress in this region increases, figures 8 a) - c), but then steadily decreases as it moves up the wall, figures 8 d) - f). This region of higher shear stress corresponds to the area of low velocity rotational flow observed in figure 5 d).

The wall shear stress between these peaks remains low for the duration of the stenosis growth. Thus it can be seen that the high wall shear stresses created by the stenosis growth is mainly concentrated in the area of the stenosis wall that breaches the interface between the regions of higher velocity central flow and the lower velocity flow near the wall. This high shear stress may play a role in the rupturing of such a stenosis growth. This is an interesting result which merits further study, the model used in this study does not have the capability to study this process however.

4.2 Pulse Cycle

It can be seen from figure 4 that the peak velocity flows presented in figures 5 and 6 only occur for a relatively brief period in the pulse cycle. For the

rest of the pulse cycle the flow velocity remains relatively low. It is, however, interesting to consider how the velocity and shear stress changes over a pulse period. This is shown in figure 7 which show the velocity and shear stress at selected times for the maximum level of stenosis.

At times $t = 0.17$ s and $t = 0.22$ s in figures 5 e) - f) and 5 g) - h) respectively, large regions of rotational flow are observed. These regions occur after the peak velocity flow and were also observed for the unstenosed case. The region of rotational flow occurs upstream of the stenosis and remains relatively fixed before completely dissipating before the next pulse cycle. The upper part of the large region seen in figure 5 e) does, however, break away and move further up the ICA.

The majority of the high shear stress is concentrated near the walls of the artery. It is observed that higher shear stresses were always present around the point of bifurcation in the artery. High shear stress was also present along the walls of the ECA for a large part of the pulse cycle. The regions of rotational observed also created patches of higher shear stress in the central region of the ICA. Low wall shear stress was prevalent for most of the pulse cycle in the CCA The right hand wall of the ICA also had large regions of low wall shear stress during most of the pulse cycle. The largest areas high shear stress along the wall of the ICA occurred near the times of peak velocity flow.

5 Conclusion

Despite the 2 dimensional nature of the model, results for the peak near wall shear compared well with literature values. Regions of low velocity, rotational flow and low near wall shear are observed in areas of the unstenosed artery known to be susceptible to atherosclerosis. These regions persist during the simulated stenosis growth as well as during the pulse cycle, suggesting that growing stenosis maintain conditions in the artery which can further promote their growth. In particular, a small region of rotational flow is observed just upstream of the upper edge of the implemented stenosis. This may increase the particle residency time for lipids and blood cells in this region and further promote stenosis progression.

High shear along the wall of the stenosis is observed when the wall of the stenosis penetrates into the higher velocity central flow, a factor that may be relevant when studying the events leading to plaque rupture and ischaemic stroke.

These results show the promise of the LBM for arterial blood-flow simulation and in particular its possible application to the further study of the haemodynamic influences on atherosclerotic progression and plaque rupture.

Future directions for this work include a 3 dimensional implementation of the LBM. The local nature of the LBM also makes it ideal for parallel implementation enabling 3 dimensional simulations to be performed.. More realistic artery conditions such as compliant walls (Fang *et al.* 2002) and red blood cells (Li *et al.* 2004a) can also be added. These areas will be the focus of continuing work in this area.

Acknowledgements

This work was partially supported by the EPSRC (UK) under Grant No. GR/N16778, Sigma Xi Grant no. 10040015 and the Australian Postgraduate Award (APA), this assistance is gratefully acknowledged.

References

Agarwal, R K, Yun, K-Y and Balakrishnan R Beyond Navier-Stokes: Burnett equations for flows in continuum-transition regime *Phys. Fluids* **13** 3061–85.

Artoli A M, Kandhai D, Hoefsloot H C J, Hoekstra A G and Sloop P M A 2004 Lattice BGK simulations of flow in a symmetric bifurcation *Future Gener. Comp. Sy.* **20** 909–916.

Asakura T and Karino T 1990 Flow Patterns and Spatial Distribution of Atherosclerotic Lesions in Human Coronary Arteries *Circ. Res.* **66** 1045–66

Bellerman R G and Sloot P M A 2001 Simulated vascular reconstruction in a virtual operating theatre *CARS 2001: Computer Assisted Radiology and Surgery* (Elsevier Science) p938–44

Bhatnagar P L, Gross E P and Krook M 1954 A model for collision processes in gases I: small amplitude processes in charged and neutral one-component system *Phys. Rev.* **94** 511–25

Boyd J, Buick J M, Cosgrove J A and Stansell P 2004 Application of the lattice Boltzmann method to arterial flow simulation: Investigation of boundary conditions for complex arterial geometries *Australas. Phys. Eng. Sci. Med.* **27** 147–52

Chen S, Chen H, Martinez D and Matthaues W 1991 Lattice Boltzmann Model for Simulation of Magnetohydrodynamics **67** 3776–9

Chen S and Doolen G D 1998 Lattice Boltzmann method for fluid flows *Annu. Rev. Fluid Mech.* **30** 329–64

Cosgrove J A, Buick J M, Tonge S J, Munro C G, Greated C A and Campbell D M 2003 Application of the lattice Boltzmann method to transition in oscillatory channel flow **36** 2609–20

Fang H, Lin Z and Wang Z 1998 Lattice Boltzmann simulation of viscous fluid systems with elastic boundaries *Phys. Rev. E* **57** R25–R28

Fang H, Wang Z, Lin Z and Liu M 2002 Lattice Boltzmann method for simulating the viscous flow in large distensible blood vessels *Phys. Rev. E* **65** Article no. 051925

Gnasso A, Irace C, Carallo C, De Franceschi M S, Motti C, Mattioli P L and Pujia A 1997 In Vivo Association Between Low Wall Shear Stress and Plaque in Subjects With Asymmetrical Carotid Atherosclerosis *Stroke* **28** 993–8

Guo Z, Zheng C and Shi B 2002 An extrapolation method for boundary conditions in lattice Boltzmann method *Phys. Fluids* **14** 2007–10

Hoekstra A G, van't Hoff J, Artoli A M, Sloop PMA 2004. Unsteady flow in a 2D elastic tube with the LBGK method *Future Gener. Comp. Sy.* **20** 917-924.

Holdsworth D W, Norley C J D, Frayne R, Steinman D A and Rutt B K 1999 Characterisation of common carotid artery blood-flow waveforms in normal human subjects **20** 219–40

Krafczyk M, Cerrolaza M, Schulz M and Rank E 1998 Analysis of 3D transient blood flow passing through an artificial aortic valve by lattice-Boltzmann methods *J. Biomech.* **31** 453–62

Krafczyk M, Tolke J, Rank E and Schulz M 2001 Two dimensional simulation of fluid-structure interaction using lattice-Boltzmann methods *Comp. Struct.* **79** 2031–7

Ku D N, Giddens D P, Zarins C K and Glagov S 1985 Pulsatile Flow and Atherosclerosis in the Human Carotid Bifurcation: Positive Correlation between Plaque Location an Low and Oscillating Shear Stress *Atherosclerosis* **5** 293–302

Ladd A J C and Verberg R 2001 Lattice Boltzmann simulations of solid particle-fluid suspensions *J. Stat. Phys.* **104** 1191–251

Li H, Fang H, Lin Z, Xu S and Chen S 2004a Lattice Boltzmann simulation on particle suspensions in a two-dimensional symmetric stenotic artery *Phys. Rev. E* **69** 031919.

Li H, Lu X, Fang H and Qian Y 2004b Force evaluation in lattice Boltzmann simulations with moving boundaries in two dimensions *Phys. Rev. E* **70** 026701.

Li H, Lu X, Fang H and Lin Z 2005 Simulation of multi-particle suspensions in a quasi-two-dimensional symmetric stenotic artery with lattice Boltzmann method *Prog. Comp. Fluid dynam.* **5** 65–74.

Lim C Y, Shu C, Niu X D and Chew Y T 2002 Application of lattice Boltzmann method to simulate microchannel flows *Phys Fluids* **14** 2299–308.

McDonald D A 1960 *Blood Flow in Arteries* Edward Arnold(Publishers) LTD

Malek A M, Alper S L and Izumo S 1999 Hemodynamic Shear Stress and its Role in Atherosclerosis *J. Amer. Med. Assoc.* **282** 2035–42

Manwart C, Aaltosalmi U, Koponen A, Hilfer R and Timonen J 2002 Lattice-Boltzmann and finite-difference simulations for the permeability for three -dimensional porous media *Phys. Rev. E* **66** Article no. 016702

Migliorini C, Qian Y, Chen H, Brown E B, Jain R K and Munn L L 2002 Red blood cells augment leukocyte rolling in a virtual blood vessel *Biophys. J.* **83** 1834–41.

Neal, M. 2002. *A study of the brass instrument lip reed mechanism using artificial lips and lattice Boltzmann flow simulation*, p 106-107. PhD Thesis, The University of Edinburgh.

Nie X, Doolen G D and Chen S 2002 Lattice-Boltzmann simulations of fluid flows in MEMS *J. Stat. Phys.* **107** 279–89.

Perktold K, Resch M and Florian H 1991 Pulsatile Non-Newtonian Flow Characteristics in a Three-Dimensional Human Carotid Bifurcation Model *J. Biomech. Eng.* **113** 464–75

Quarteroni A, Tuveri M and Veneziani A 2000 Computational vascular fluid dynamics: problems, models and methods *Comput. Visual Sci.* **2** 163–97

Quian Y H, d'Humieres D and Lallemand P 1992 Lattice BGK Models for Navier-Stokes Equation *Europhys. Lett.* **17** 479–84

Shan X and Chen H 1993 Lattice Boltzmann Model for Simulating Flows with Multiple Phases and Components *Phys. Rev. E* **47** 1815–9

Spaid M A A and Phelan Jr. F R 1997 Lattice Boltzmann methods for modeling microscale flow in fibrous porous media *Phys. Fluids* **9** 2468–74.

Steinke W, Els T and Hennerici M 1994 Compensatory Carotid Artery Dilation in Early Atherosclerosis *Circulation* **89** 2578–81

Sun C H, Migliorini C and Mun L L 2003 Red blood cells initiate leukocyte rolling in postcapillary expansions: A lattice Boltzmann analysis *Biophys. J.* **85** 208–22.

Tamagawa M and Matsuo S 2004 Predictions of thrombus formation using lattice Boltzmann method - (Modeling of adhesion force for particles to wall) *JSME Int. J. C* **47** 1027–34.

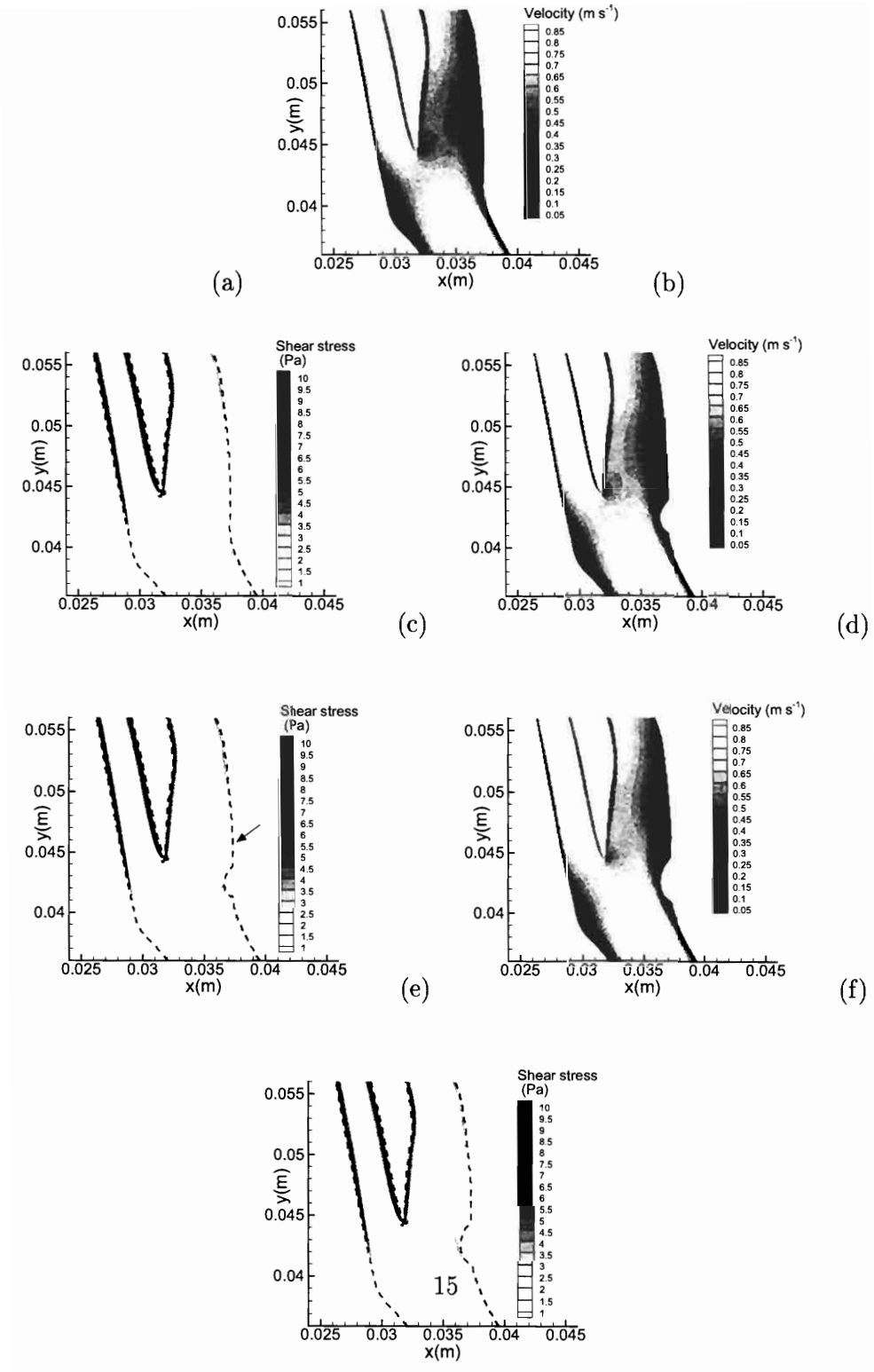

Figure 5: Velocity and shear stress fields in response to implemented stenosis growth. Unstenosed artery (**a-b**), stenosis increments 10 (**c-d**) and 15 (**e-f**) shown. The artery wall is represented by the dashed line in the shear stress

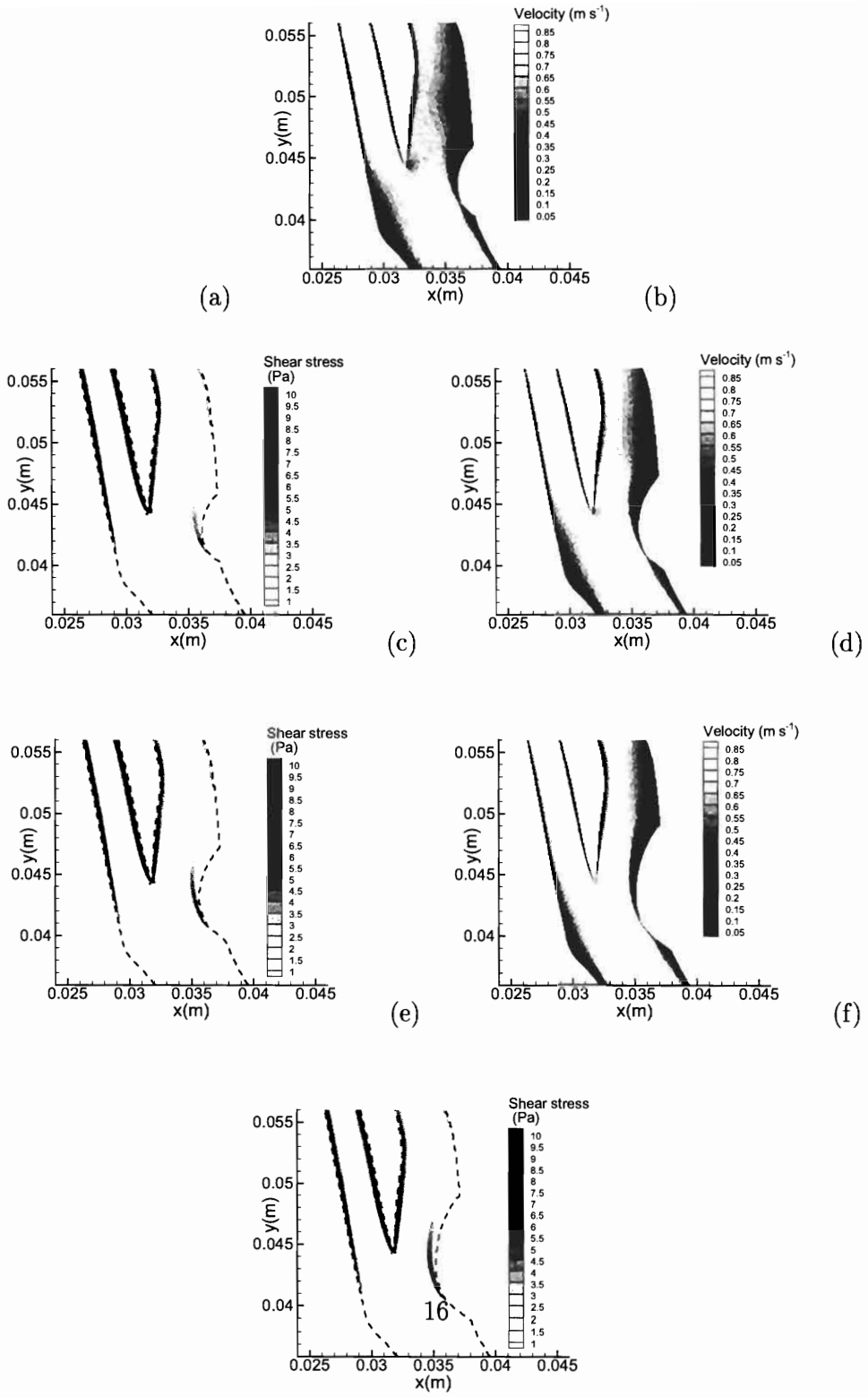

Figure 6: Velocity and shear stress fields in response to implemented stenosis growth. Stenosis increments 20 (**a-b**), 25 (**c-d**) and 30 (**e-f**) shown. The artery wall is represented by the dashed line in the shear stress graphs.

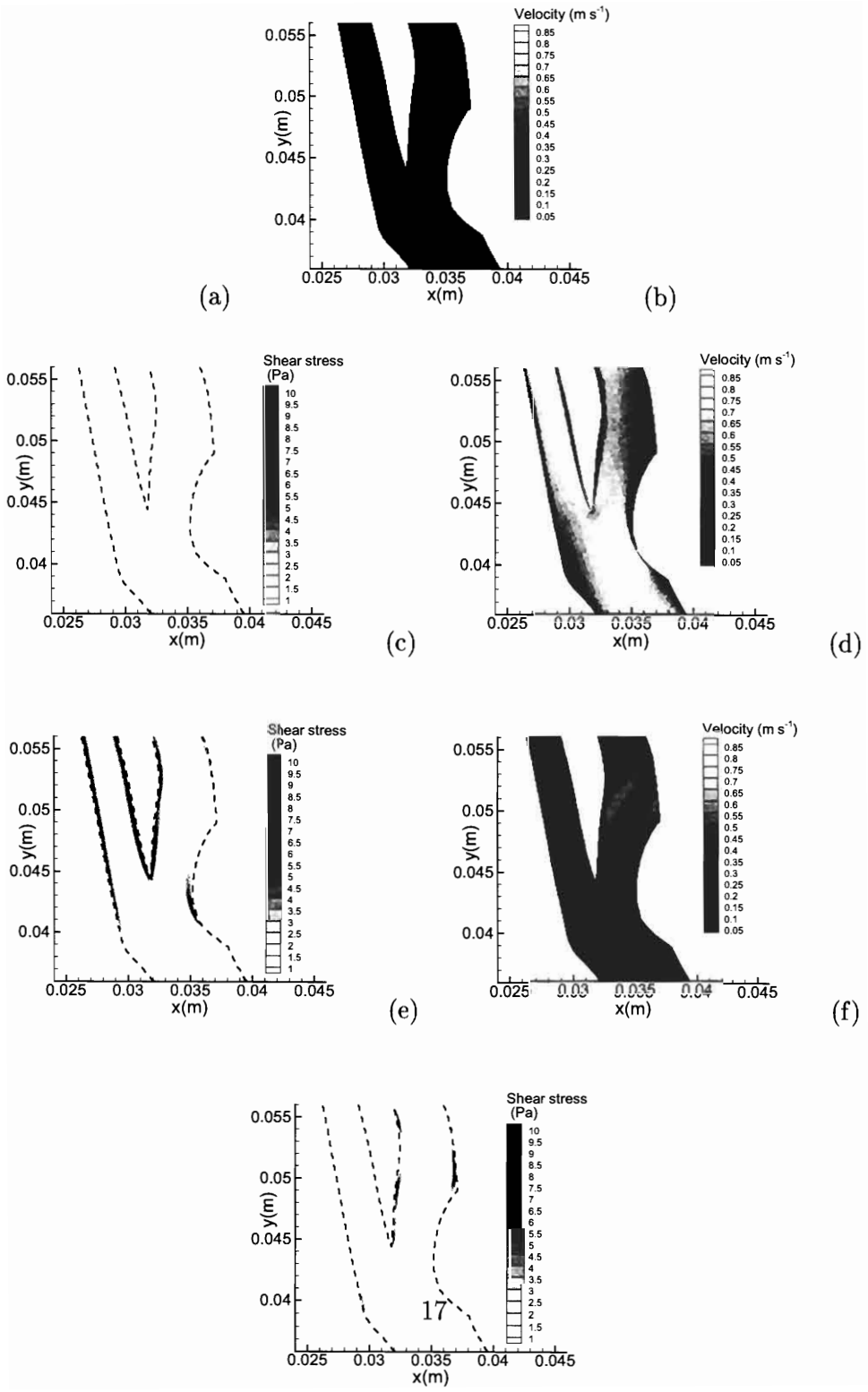
Velocity (m s-1)
Shear stress (Pa)
y(m)
x(m)
(a)
(b)
(c)
(d)
(e)
(f)

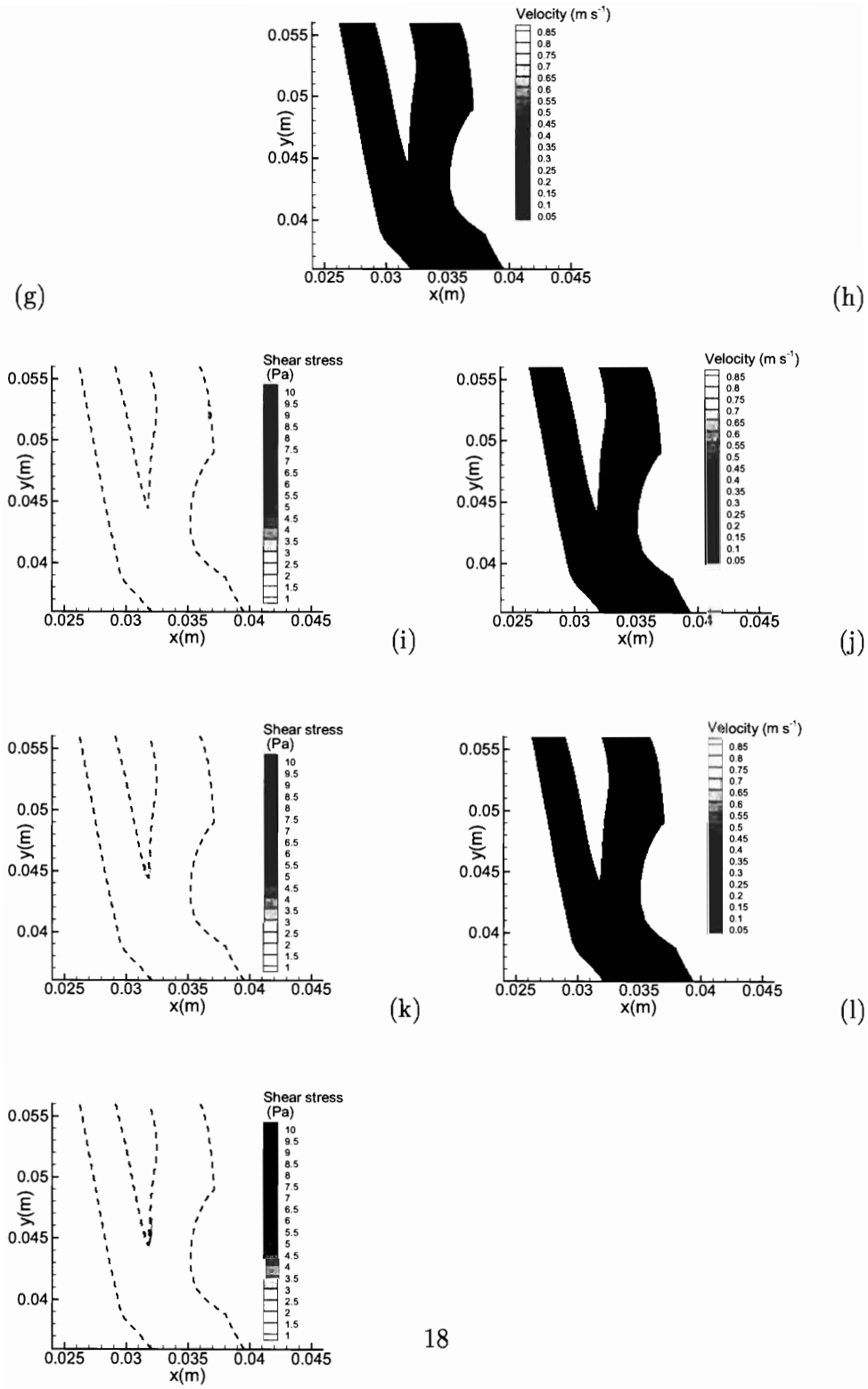

Figure 7: Velocity and shear stress during pulse cycle for maximally stenosed artery. (**a-b**) $t = 0.05$ s, (**c-d**) $t = 0.12$ s and (**e-f**) $t = 0.17$ s, (**g-h**) $t = 0.22$ s, (**i-j**) $t = 0.28$ s, (**k-l**) $t = 0.50$ s. The artery wall is represented by the dashed line in the shear stress graphs. Velocity and shear stress fields during

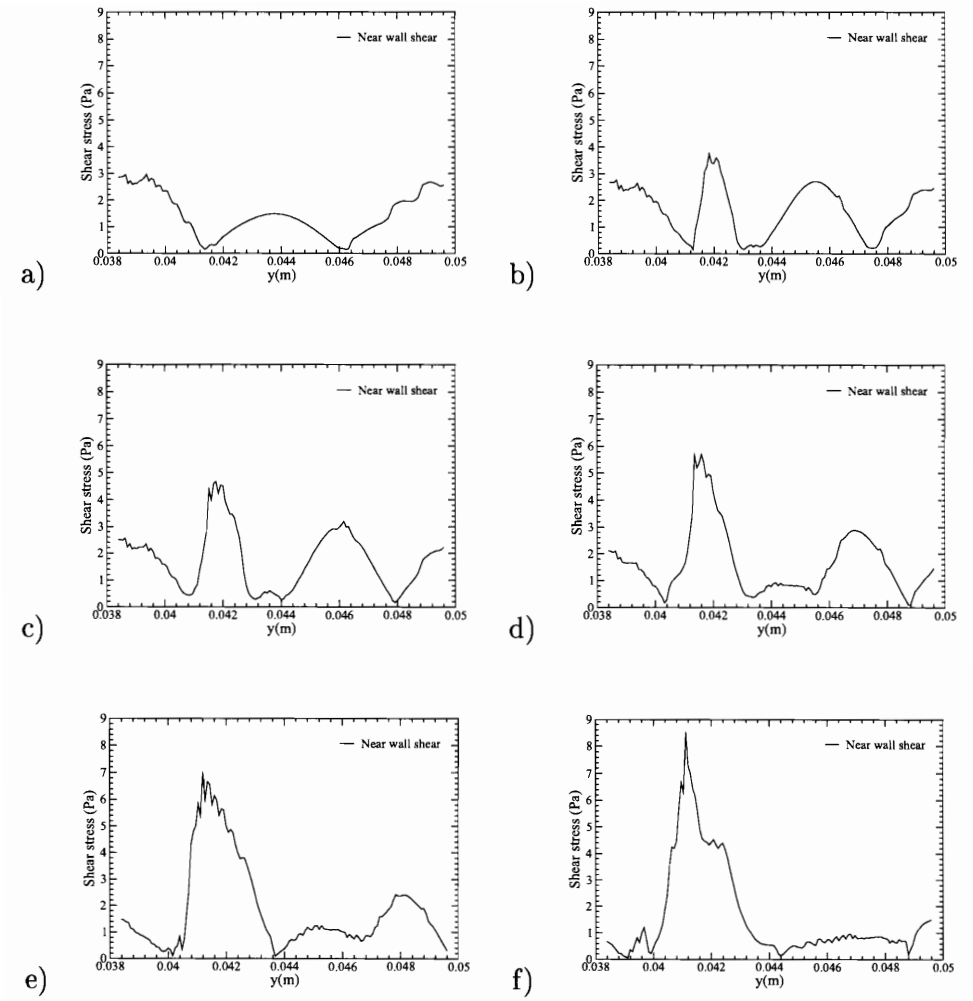

Figure 8: Response of near wall shear stress to stenosis growth, increments a) 0, b) 10, c) 15, d) 20, e) 25, and f) 30 shown. Shear stress two grid-lengths from the wall shown.